JOURNAL OF GEOPHYSICAL RESEARCH, VOL. 113, A11214, doi:10.1029/2008JA013635, 2008

Click Here for Full Article

# Rice Convection Model simulation of the 18 April 2002 sawtooth event and evidence for interchange instability

J. Yang,[1] F. R. Toffoletto,[1] R. A. Wolf,[1] S. Sazykin,[1] R. W. Spiro,[1] P. C. Brandt,[2] M. G. Henderson,[3] and H. U. Frey[4]

Received 22 July 2008; revised 21 September 2008; accepted 30 September 2008; published 20 November 2008.

[1] We present the results of a Rice Convection Model (RCM) simulation of the 18 April 2002 sawtooth event. This event occurred as a series of quasi-periodic substorms during fairly stable solar wind conditions. It is modeled by (1) prescribing a solar-wind-driven magnetic field model (T01_s) augmented by additional current loops representing the magnetic effects of the substorm current wedge and (2) by carefully specifying a substorm-phase-dependent plasma distribution at the RCM outer boundary at 8 $R_e$ such that a hot and attenuated plasma distribution is used after every substorm onset. The set of input parameters was adjusted to make the simulation results agree with the primary signatures of the sawtooth event, specifically the sequence of magnetic field stretching and dipolarization observed by the GOES spacecraft and the associated sharp increases and gradual decreases in the flux of energetic protons measured by the LANL/Synchronous Orbit Plasma Analyzer (SOPA) instruments on other geosynchronous spacecrafts. The results suggest the important role that higher temperature and lower density plasma-sheet plasma plays in producing flux enhancements at geosynchronous orbit. The results also confirm that induction electric fields associated with magnetic field collapse after substorm onsets can serve as a likely mechanism for the energization of particles up to 25 keV. Synthetic high-energy neutral atom images are compared with IMAGE/HENA measurements for 10–60 keV hydrogen atoms. Magnetic field dipolarization over a large range of local time resulted in a dramatic reduction in the plasma entropy parameter $PV^{5/3}$ on the boundary. The simulation indicates that the ring current intensified 10–20 minutes after every onset, associated with the injection of low $PV^{5/3}$ flux tubes through the boundary. The low $PV^{5/3}$ plasma also produced an interchange convection in the inner magnetosphere, which drives Birkeland currents in a quasi-periodic upward-downward pattern with a lifetime of 40–60 minutes and spatial extent of 1.5–2.0 hours. The results suggest that the spatial quasi-periodic and nearly north–south-aligned auroral arcs observed by an IMAGE/FUV WIC detector might be caused by interchange instability.

**Citation:** Yang, J., F. R. Toffoletto, R. A. Wolf, S. Sazykin, R. W. Spiro, P. C. Brandt, M. G. Henderson, and H. U. Frey (2008), Rice Convection Model simulation of the 18 April 2002 sawtooth event and evidence for interchange instability, *J. Geophys. Res.*, *113*, A11214, doi:10.1029/2008JA013635.

## 1. Introduction

[2] Sawtooth events are generally identified as quasi-periodic oscillations of energetic particle fluxes at geosynchronous orbit [*Borovsky et al.*, 1993; *Belian et al.*, 1995]. They usually occur during storm times, with a periodicity of approximately 2–4 hours and can last for up to 5–8 cycles [*Huang et al.*, 2003a; *Henderson et al.*, 2006]. By analyzing solar wind conditions, *Huang et al.* [2003b] and *Henderson et al.* [2006] found that sawtooth events can occur under fairly stable solar wind conditions characterized by a continuous southward IMF $B_z$. However, *Lee et al.* [2004] interpreted every sawtooth onset as the result of a solar wind pressure enhancement. While their triggering mechanism(s) are still the subject of some debate, sawtooth events are generally viewed as a series of quasi-periodic substorms. *Huang et al.* [2003b] analyzed Geotail data during two sawtooth events, concluding that there were near-tail reconnections and plasmoid formations with a mean period of ~2.7 hours. *Henderson* [2004] re-examined the CDAW-9C interval and analyzed it as a sawtooth event, which placed tail reconnection inside −11 $R_e$. During sawtooth events magnetic field stretching and dipolarization can be very strong in both the nightside and dusk sectors [*Pulkkinen et al.*, 2006].

[1]Department of Physics and Astronomy, Rice University, Houston, Texas, USA.
[2]Applied Physics Laboratory, Johns Hopkins University, Laurel, Maryland, USA.
[3]Los Alamos National Laboratory, Los Alamos, New Mexico, USA.
[4]Space Sciences Laboratory, University of California, Berkeley, California, USA.

Copyright 2008 by the American Geophysical Union.
0148-0227/08/2008JA013635$09.00

[3] During a substorm, the magnetospheric magnetic field can be very dynamic and plasma quantities are highly variable. During the growth phase, the field in the magnetotail stretches and the plasma sheet thins. In the subsequent expansion phase, the field collapses to a more dipole-like configuration, which may be associated with the development of a substorm current wedge as suggested by *McPherron et al.* [1973]. *Tsyganenko* [1997] developed an empirical model to describe the magnetic field produced by the current wedge.

[4] In the convection picture of magnetospheric substorm dynamics, after substorm onset, conservation of the specific entropy parameter ($PV^{5/3}$) is violated, where $P$ is plasma pressure and $V$ is the flux tube volume per unit magnetic flux. Both the near Earth X-line model of a substorm [*Hones*, 1977] and the cross-tail current disruption model [*Lui et al.*, 1992] suggest the creation of a dipolarized bubble, which reduces the flux tube volume dramatically. *Wolf et al.* [2006b] estimated the specific entropy of flux tubes at around $-10$ $R_e$ during two substorms, finding that $PV^{5/3}$ was reduced by a factor of 2–3 after onset. *Lemon et al.* [2004] simulated an idealized storm with a depletion channel of low $PV^{5/3}$, leading to an injection of plasma-sheet plasma into the ring current. Since sawtooth event plasma injections are typically very wide in local time and occur almost simultaneously all around geosynchronous orbit [*Huang et al.*, 2003b; *Reeves et al.*, 2004], and since each injection is associated with the escape of a plasmoid [*Huang et al.*, 2003b], it is plausible to assume that $PV^{5/3}$ is reduced in the plasma sheet over a wide range of local times. On the other hand, even when $PV^{5/3}$ is conserved, *Kaufmann and Paterson* [2006] found that field stretching and dipolarization change the plasma temperature, density and pressure of a flux tube. Yet another important substorm-associated process that could influence plasma-sheet plasma parameters is ionospheric outflow. The ion outflow rate can be as large as $10^{25}$ ions $s^{-1}$ [*Yau et al.*, 1985] in total, and $10^{22}$ to $10^{24}$ ions $s^{-1}$ during ion conic events near the auroral/polar cap boundary, and remain for up to 90 minutes after substorm onset at this high level [*Tung et al.*, 2001]. Ion outflow would tend to make the plasma sheet population colder and denser in the substorm recovery phase [*Wing et al.*, 2007]. Cold plasma can also enter the plasma sheet via the low-latitude boundary layer [*Fujimoto et al.*, 1998].

[5] Simulations of the 18 April 2002 event have been carried out using different techniques. *Goodrich et al.* [2007] investigated the magnetospheric responses to steady solar wind conditions using global MHD simulations (LFM), finding that the reconnection in the midtail is intermittent and patchy in sawtooth event, while the reconnection in the steady magnetospheric convection (SMC) is quasi steady. *Kuznetsova et al.* [2007] modified the MHD Ohm's law in the regions of likely reconnection to include nongyrotropic pressures, which could reproduce quasi-periodic reconnections when driven by a steady southward IMF. With this modification, *Taktakishvili et al.* [2007] modeled the ring current buildup and the oscillation of energetic flux at geosynchronous orbit by coupling the BATS-R-US code and the Fok Ring Current Model, providing a detailed picture of inner-magnetospheric particles, on the basis of MHD-computed electric and magnetic fields.

[6] In this paper, we present results from a Rice Convection Model (RCM) simulation of the 18 April 2002 sawtooth event. Our approach is to impose quasi-periodic boundary conditions on the plasma number density, temperature, and entropy parameter at the RCM outer boundary to reflect what is known about the substorm-phase-dependent phenomenology of the plasma-sheet plasma distribution as described above. Since there are no measurements available along the modeling boundary to directly constrain the RCM's plasma boundary condition, we adjust solar-wind-driven empirical plasma parameters in a reasonable range, comparing the results with multipoint observations until reasonable agreement is achieved between model results and the classic sawtooth behavior exhibited by the LANL/ Synchronous Orbit Plasma Analyzer (SOPA) data. Inputs to the magnetic field model are also adjusted for reasonable agreement with measurements by GOES magnetometers.

[7] Using prescribed magnetic field configurations, the RCM computes energy-dependent, bounce-averaged particle distribution functions as well as currents and electric fields in the closed field line region of the inner and middle magnetosphere. The RCM calculation is self-consistent, in that the effect of the particle distribution is considered in the calculation of the Birkeland current and electric potential distribution. Assuming strong-elastic-pitch-angle scattering and neglecting sources and losses, the specific entropy parameter $P_sV^{5/3}$ and the energy invariant $\lambda_s = E_sV^{2/3}$, are conserved along the drift path, where $P_s$ is the partial pressure for a given value of $\lambda_s$ and $E_s$ is particle kinetic energy. By defining the number of particles per unit magnetic flux $\eta_s$ with invariant $\lambda_s$, the plasma number density $N$, temperature $T$, and entropy parameter $PV^{5/3}$ can be written as

$$N = \frac{\sum_s \eta_s}{V}$$

$$T = \frac{\frac{2}{3}V^{-\frac{2}{3}}\sum_s \lambda_s\eta_s}{\sum_s \eta_s}$$

$$PV^{\frac{5}{3}} = \frac{2}{3}\sum_s \lambda_s\eta_s$$

Detailed descriptions and applications of the RCM have been given by *Wolf* [1983] and *Toffoletto et al.* [2003].

[8] Section 2 reviews observations of the 18 April 2002 sawtooth event. Since the magnetic field configuration and plasma distribution are important inputs to the RCM, section 3 focuses on how we specify both the magnetic field within the simulation region and plasma boundary conditions at the RCM outer boundary. Section 4 demonstrates the degree to which we were able to adjust boundary conditions to fit GOES and LANL/SOPA data; model predictions are then compared with other data sets, namely, lower-energy particle fluxes measured by LANL/MPA, 10–60 keV fluxes from IMAGE/HENA, and auroral patterns from IMAGE/FUV.

## 2. Observational Overview of the 18 April 2002 Sawtooth Event

[9] The 18 April 2002 sawtooth event occurred during a two-day long magnetic storm, which began early on

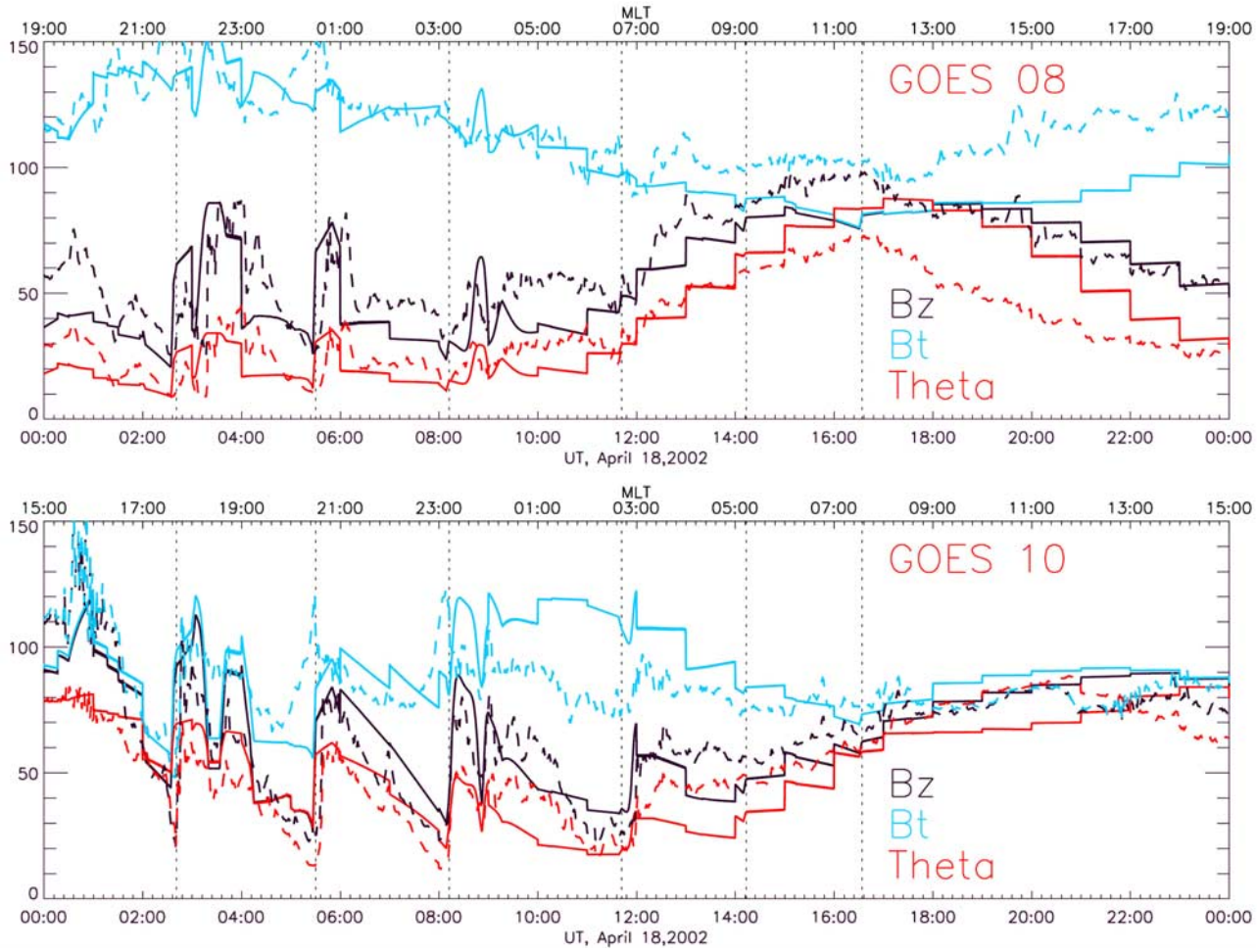


**Figure 1.** Comparison of the magnetic field observed by GOES 8 and GOES 10 at geosynchronous orbit (dashed lines) and the field given by the T01_s model and Tsyganenko-based substorm current wedge model (solid lines). The blue, black, and red dashed lines represent the total magnetic field, the Bz component, and the inclination angle in GSM coordinate. The top and bottom are for GOES 8 and GOES 10, respectively. The vertical dotted lines at 0241, 0530, 0812, 1142, 1413, and 1634 UT indicate the southward turnings of Bz and peaks of the field strength at Geotail, taken from *Huang et al.* [2003b].

17 April. This event was well covered by multiple satellite observations and has been studied extensively [e.g., *Huang et al.*, 2003b; *Henderson et al.*, 2006; *Clauer et al.*, 2006; *Ohtani et al.*, 2007; *Reeves et al.*, 2004]. During this event, the solar wind velocity had a sudden change at around 0010 UT on 18 April, followed by a number density peak at about 0100 UT. Thereafter, the solar wind velocity gradually decreased from 530 km/s to 450 km/s; the solar wind density remained fairly stable as low as 2 $cm^{-3}$; the IMF $B_z$ was continuously southward with variations from −6 to −12 nT. *Huang et al.* [2003b] identified seven teeth in the sawtooth event, beginning at around 0036, 0241, 0530, 0812, 1142, 1413 and 1634 UT respectively. The onset times were determined by analyzing the peaks of the magnetic field and the southward turnings of Bz in the magnetotail at Xgsm = −22∼−29 $R_e$, Ygsm = −7∼−14 $R_e$, Zgsm = 7∼12 $R_e$ observed by Geotail [see *Huang et al.*, 2003b, Figure 1]. In contrast, *Henderson et al.* [2006] extracted seven teeth from 0239 UT to 2104 UT, determined by the combination of electron and proton flux enhancements from LANL/SOPA detectors.

[10] High-resolution SOPA measurements, consisting of electrons in the range 50−500 keV and protons in the range 50−400 keV, show dispersionless particle flux enhancements after every onset in the dusk and midnight sector, but dispersive in the post dawn sector [*Henderson et al.*, 2006; *Reeves et al.*, 2004]. Relating the drift times of particles of different energies with the dispersive increase on the dayside, *Reeves et al.* [2004] estimated the injection boundary to extend across the nightside from the pre-dusk sector to the post-dawn sector (17−7 hours LT). *Clauer et al.* [2006] examined ground magnetograms during this event, and found the disturbance for each tooth to be similar to the disturbance associated with a typical substorm except that the sawtooth oscillations affect a wider range of local times.

[11] *Ohtani et al.* [2007] analyzed Cluster observations from 0700 to 1030 UT. At the 0812 UT onset, when Cluster located at about 4.6 $R_e$ radial distance was deep in the inner magnetosphere near 2100 MLT, the particle fluxes recorded by RAPID increased without obvious dispersion, and the *in situ* plasma movement was dominated by radial motion, because of an azimuthal induction electric field.

[12] Results of remote sensing of the inner magnetosphere and the north polar region have also been presented [e.g., *Henderson et al.*, 2006; *Huang et al.*, 2003b; *Clauer et al.*, 2006; *Ohtani et al.*, 2007]. IMAGE/HENA observations around the 1142 UT onset show westward drift and little hydrogen intensity enhancement [*Henderson et al.*, 2006]. The auroras during this event were very active and long-lasting during each tooth cycle [*Huang et al.*, 2003b]. A double oval configuration and eastward propagation of omega-band forms were also observed during this event [*Henderson et al.*, 2006]. *Ohtani et al.* [2007] characterized the auroral structure as quasi-periodic in space, after the onset at around 0812 UT.

## 3. Simulation Setup

[13] In an effort to match simulation results with observations, we have carefully adjusted the various RCM model inputs to best reflect conditions during the sawtooth event of 18 April 2002, as described below.

### 3.1. Magnetic Field Inputs

[14] The blue, black, and red dashed lines in Figure 1 show the total magnetic field, the $B_z$ component and the inclination angle in GSM coordinates observed by GOES 8 and GOES 10 in the top and bottom, respectively. The six vertical dotted lines, at 0241, 0530, 0812, 1142, 1413, and 1634 UT, represent times of southward $B_z$ turnings and total field strength peaks as identified by *Huang et al.* [2003b] from Geotail observations. As shown in Figure 1, these times correlate well with indicators of magnetic field dipolarization at geosynchronous orbit, namely, increases in total field strength, Bz, and inclination angle. Located at different magnetic local times, GOES 8 and GOES 10 detected 3 and 4 dipolarizations in the dusk and midnight sector, respectively, and no dipolarizations on the dayside. Before the sudden dipolarization, the $B_z$ component and the inclination angle decreased gradually, representing field stretching in the growth phase of substorms.

[15] In order to reproduce the storm time magnetic field and dipolarization associated with the substorm expansion phase, we combine the T01_s magnetic field model [*Tsyganenko*, 2002a, 2002b] with a substorm current wedge model based on *Tsyganenko* [1997]. The solar-wind-driven T01_s magnetic field alone does not reproduce the strong growth-phase magnetic field stretching and subsequent dipolarization, since the solar wind parameters were fairly stable and the magnetic indices Dst and Kp did not show sawtooth-like oscillations. *Tsyganenko* [1997] proposed an empirical substorm current wedge to model the dipolarized field in the substorm expansion phase. This model has two sets of wedge-like spreading currents centered at midnight, utilizing five parameters to control the shape, the angle to the equatorial plane, the spread and the amplitude of the currents. We modified the model to add a rotation parameter, allowing the wedge to be centered at any local time. We carefully adjusted input parameters for the substorm current wedge to best fit the dipolarizations observed by GOES 8 and GOES 10. Since these two satellites did not observe dipolarizations at around 1413 and 1634 UT, when they were on the dayside, we used the 1142 UT set of substorm current wedge parameters as input for the last two dipolarizations. A detailed description of the setup of the substorm current wedge model is given in Appendix A.

[16] Comparing observation and model magnetic field results, we attribute discrepancies to two main causes. First, we did not take tilt into account in our implementation of the T01_s model, since the present version of RCM assumes zero tilt angle of Earth's internal field, but the GOES satellites are assumed to be on the equatorial plane at a distance of 6.6 $R_e$ in GEO coordinate system. This discrepancy is apparent by comparing GOES 8 observations and model results from 1700 to 2400 UT. The second discrepancy is apparent from 0200 to 0800 UT when GOES 10 was in the dusk sector, where the observation shows stronger stretching prior to every onset than that given by the T01_s model. *Pulkkinen et al.* [2006] has suggested that the field stretching in the dusk sector could be as strong as on the nightside prior to sawtooth event onsets.

### 3.2. Electric Potential Distribution on the Simulation Boundary

[17] During active times, it is reasonable to assume that the plasma sheet and the injection boundary move closer to the Earth [*Mauk and Meng*, 1983]. Throughout our modeled sawtooth event interval, the Kp index remained above 6. We set the outer boundary of the RCM to be a circle of radius 8 $R_e$, which is well inside the magnetopause standoff distance which ranged from 8.5 to 11.7 $R_e$ as calculated using observed solar wind parameters, following *Shue et al.* [1998]. We suspect that a more distant boundary would require a more sophisticated treatment of the electric potential distribution at the boundary in combination with the substorm current wedge magnetic field model to insure the characteristic dispersionless sawtooth pattern observed; this will be left for further study.

[18] The total polar cap potential drop (PCP) calculated using the Boyle formula [*Boyle et al.*, 1997] varies in the range from 100 to 144 kV. In the period when the magnetic field is stretching, we scale the total PCP by the ratio 8.0/magnetopause-standoff-distance to estimate the potential drop across the 8 $R_e$ region. When the field dipolarizes, we apply the total PCP across the 8 $R_e$ region. The plasma inflow region corresponds to the region of westward electric field on the RCM boundary, adjusted to match the dusk and dawn bounds for the first four injections as given by *Reeves et al.* [2004], i.e., the inflow regions were from 1500 to 0100 MLT for the 0241 UT injection, from 1400 to 0700 MLT for the 0530 UT injection, from 1400 to 0100 MLT for the 0812 UT injection, and from 1800 to 0100 MLT for the 1142 UT injection, respectively. The last two plasma inflow boundaries are assumed to be the same as that at 1142 UT.

### 3.3. Plasma Distribution on the Boundary

[19] Using the *Tsyganenko and Mukai* [2003] empirical model, which relates solar wind and IMF parameters to the temperature and number density of the central plasma sheet from $-10$ to $-50$ $R_e$, we calculate the plasma sheet temperature (*Tps*) to range from 8 to 10 keV and number density (*Nps*) to range from 0.19 to 0.53 $cm^{-3}$, at $-10$ $R_e$ during the period of relatively stable solar wind conditions after 0200 UT. *Borovsky et al.* [1998] fitted plasma sheet parameters with data at geosynchronous orbit and 11.5–22.5 $R_e$ in the neutral sheet to power law functions of radius *r*.

Using the power law dependence given by *Borovsky et al.* [1998], $N \sim (r/Re)^{-1.38}$, $T \sim (r/Re)^{-0.56}$, we determine the plasma sheet $T = (0.8)^{-0.56}*Tps \sim 8.5-11.5$ keV and $N = (0.8)^{-1.38}*Nps \sim 0.24-0.70$ cm$^{-3}$ at the $-8$ $R_e$ RCM simulation boundary. However, these statistical models alone cannot be expected to fully reflect plasma sheet parameter variations during a sawtooth event. Therefore during one tooth cycle, from the beginning of the field dipolarization to the end of the field stretching, we take substorm-related processes into account by substantially modifying the above statistical plasma sheet temperature and number density estimations.

[20] *Wing et al.* [2007] showed that, during both the substorm growth phase and recovery phase, the plasma sheet number density near $-8$ to $-10$ $R_e$ could be 2–3 times larger than that during the expansion phase. The denser plasma sheet is associated with ion outflow from the auroral zone [*Yau et al.*, 1985; *Tung et al.*, 2001]. Normally the ion outflow peaks 20–30 minutes after substorm onset, and lasts as long as 90 minutes [*Wilson et al.*, 2004]. The auroral activity associated with each tooth cycle during this event was extremely intense and long [*Huang et al.*, 2003b; *Henderson et al.*, 2006], resulting in a substantially denser plasma sheet during the recovery and growth phase than that during expansion phase. Therefore we set the plasma number density at the boundary just before the substorm onset as $N = 2.73*(0.8)^{-1.38}*Nps$. After the substorm onset, the plasma density within the current wedge is significantly decreased [*Lyons et al.*, 2003]. Therefore we set the plasma number density on the boundary just after the substorm onset as $N = 1.33*(0.8)^{-1.38}*Nps$, which is a reduction by a factor of 2 compared with the pre-onset condition.

[21] Plasma temperature enhancements after substorm onset have been attributed to reconnection and induction electric field acceleration. *Lyons et al.* [2003] associated the temperature increase and flux enhancement after substorm onset with compression of the magnetic field within the dipolarization current wedge. The induction electric field due to the magnetic field collapse tends to accelerate particles, which is actually equivalent to adiabatic compression if the energy invariant is conserved during the field collapse [*Wolf et al.*, 2006a]. Therefore the plasma temperature on the boundary just before every onset is set as $T = (0.8)^{-0.56}*Tps$; while the plasma temperature on the boundary just after substorm onset is 2 times higher than that, i.e., $T = 2.0*(0.8)^{-0.56}*Tps$.

[22] The conservation of $PV^{5/3}$ is violated by reconnection in the plasma sheet. The stretched closed flux tube collapses into a dipole-like closed field line with smaller flux tube volume, plus an escaping plasmoid. *Wolf et al.* [2006b] estimated that the flux tube volume could decrease by a factor of 2 during substorm expansion phase. The RCM cannot self-consistently represent the effects of reconnection and/or other processes that violate the adiabatic drift laws, processes that apparently play a vital role in substorm and sawtooth events. Thus we place the outer boundary of our calculation earthward of those processes and represent their influence on the inner magnetosphere in terms of boundary conditions. We use the RCM to model the inner magnetospheric effects of the sawtooth event, not the sawtooth event *per se*. During this sawtooth event Geotail detected quasi-periodic strengthening of magnetic field and southward turning of $B_z$ component in the magnetotail (Xgsm = $-22\sim-29$ $R_e$, Ygsm = $-7\sim-14$ $R_e$, Zgsm = $7\sim12$ $R_e$), which implies that there were quasi-periodic reconnections and plasmoid escapes in the plasma sheet [*Huang et al.*, 2003b]. However, the amount of flux tube volume reduction in every expansion phase is uncertain and impossible to directly measure by one spacecraft. For the results presented here, the flux tube volume reduction factor on the boundary is taken to be 2.0, which was determined by trial and error.

[23] Taking these processes into account, two sets of plasma distributions on the model boundary are used for every tooth cycle. At the end of the substorm growth phase, we set the distribution function to be a double Maxwellian function [*Borovsky et al.*, 1998]: a cooler Maxwellian with $T = (0.8)^{-0.56}*Tps$ and $N = 2.73*(0.8)^{-1.38}*Nps$, and a hotter Maxwellian with $5T$ and $0.0003N$, which contributes less than 0.5% to the total plasma pressure. With the T01_s model, we compute the flux tube volume $V$ at $-10$ $R_e$ at midnight, to complete the setup of the distribution function of $\eta_s(\lambda_s)$. We set the distribution function as a $\kappa = 2$ distribution just after the substorm onset, with $T = 2.0*(0.8)^{-0.56}*Tps$ and $N = 1.33*(0.8)^{-1.38}*Nps$, but with the nonadiabatically reduced flux tube volume $0.5V$. We set the plasma boundary at $-8$ $R_e$, and the plasma distribution on the boundary during the whole cycle of one tooth is found by interpolation between these two distributions. For this simulation, since there were no plasma parameter measurements at $\sim8$ $R_e$ on the night side, those factors were mainly determined by making a number of runs and comparing RCM-calculated geosynchronous fluxes with LANL/SOPA observations. Reasonable changes were made in this set of parameters until the results were qualitatively consistent with the observations. The plasma parameters at the center of the inflow boundary are plotted as a function of time in Figure 2. The number density of electrons on the boundary is set equal to the number density of protons, and the electron temperature is a factor of 7.8 lower than the proton temperature, following *Baumjohann et al.* [1989]. The ratio of the number density of oxygen ions to protons is based on the AE index, following *Daglis et al.* [1994], assuming the two ion species have the same temperature.

## 4. Simulation Results and Discussions

### 4.1. Energetic Proton Flux at Geosynchronous Orbit

[24] Figure 3 compares model results (left) with observed geocentric proton fluxes in four different energy bands from five different satellites. Since the RCM assumes the dipole axis to be untilted, the five geosynchronous satellites in the model are confined on the equatorial plane at a distance of 6.6 $R_e$ from the Earth. The simulation results (left) are consistent with the observations (right) both in shape and magnitude, indicating sudden enhancement in flux after every onset and subsequent gradual decline. We also computed the partial pressure for particles having energies less than 45 keV at the geosynchronous orbit, which is varying in the range of 0.3–5 nPa, consistent with the 0.3–4 nPa variations observed by the MPA detector. Figure 4 shows the particle moments observed by 1991–080 MPA instrument for the whole day and the corresponding simulated results, which indicates rough qualitative agreement espe-

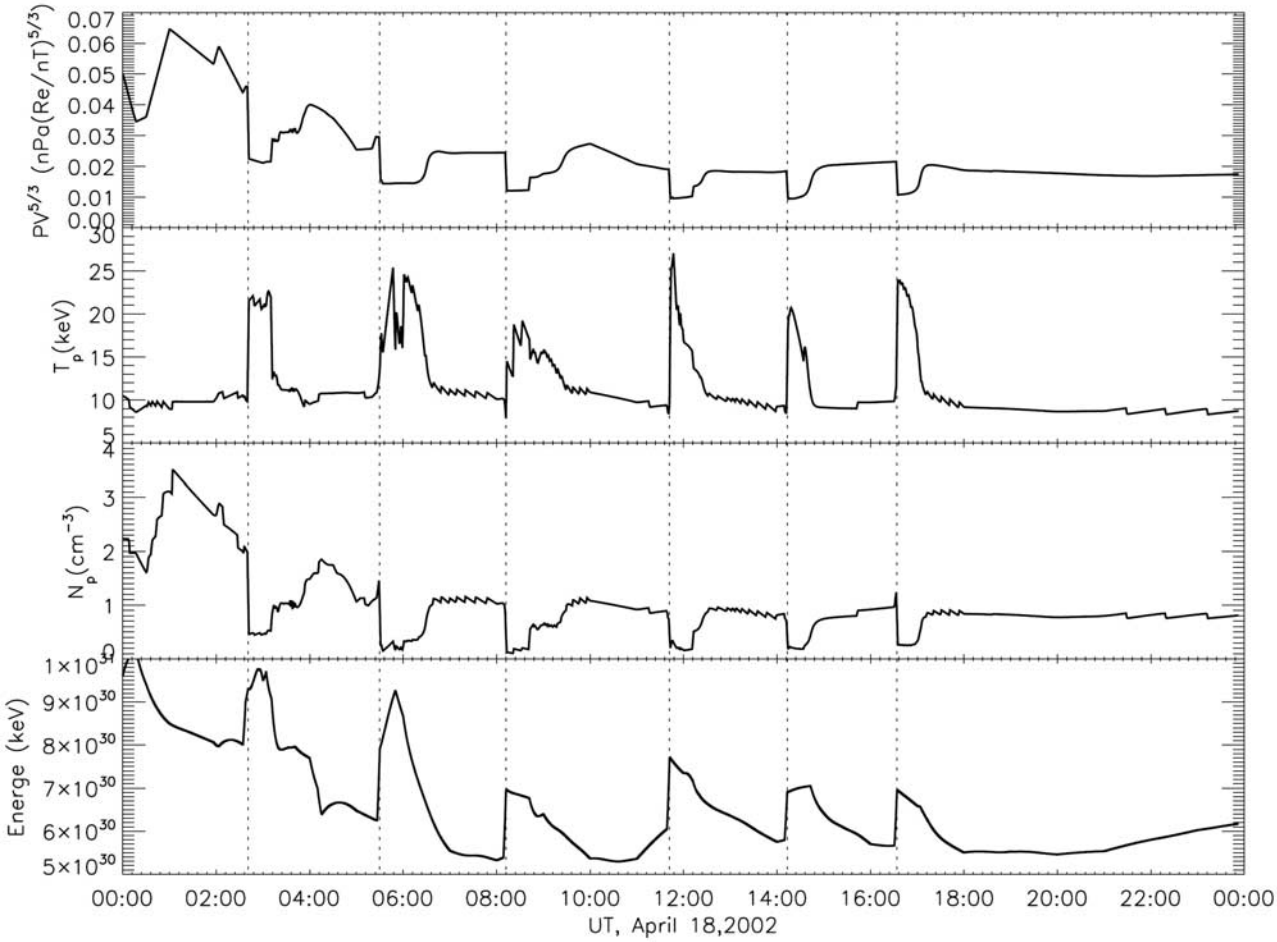


**Figure 2.** The time-dependent proton number density $N_p$, proton temperature $T_p$, and the total entropy parameter $PV^{5/3}$ at the center of the inflow boundary. The bottom shows the total energy of particles within the simulation region. The vertical dotted lines are at the same times as in Figure 1.

cially for electron number density, proton number density, proton temperature and particle pressure. Since we set the electron temperature/proton temperature ratio to be fixed at 1/7.8 on the simulation boundary, the modeled electron temperature may be dramatically lower than observation for some periods of time. From the viewpoint of the simulation, the rapid increase in flux is mainly contributed by the injection from the boundary of $\kappa = 2$ and T $\sim$ 25 keV plasma, which has a high-energy tail. To best match the SOPA observation, we find that a high-temperature plasma distribution is needed and the 25 keV temperature of plasma in the near-Earth plasma sheet at 8 $R_e$ is much higher than the usual 5–15 keV during quiet and some active times. One interesting and controversial question from this simulation is: Could the ion temperature at $-8$ $R_e$ just after substorm onset be as high as 25 keV? If so, what mechanism could energize the particles to that high temperature? One possibility is that the electric field induced by the magnetic field collapse accelerates the particles outside the simulation boundary. *Pulkkinen et al.* [2006] associated sawtooth injections with strong stretching and dipolarization in both the dusk and midnight sectors. Suppose that a field line which was stretched in the substorm growth phase with a crossing point at $-20$ $R_e$ (T89, Kp = 4) collapsed to a dipole-like field with a crossing point at $-7$ $R_e$ (T89, Kp = 1) after onset within 1 minute. The induction electric field could be estimated from Faraday's Law, E $\sim$ dB/dt*L $\sim$ (10 nT/60 s)*5 $R_e$ $\sim$ 5 mV/m. The particles could be easily accelerated to an energy of tens of keV by nonadiabatic process [*Delcourt*, 2002].

### 4.2. IMAGE/HENA Flux and the Ring Current

[25] Figure 5 shows energetic neutral atom fluxes observed by IMAGE/HENA and the corresponding synthetic flux calculated from the simulation for the third tooth cycle, beginning with the jump of $B_z$ in the tail that was detected by Geotail at 0812 UT. To synthesize the flux from the RCM simulation, we assume a virtual detector at the same location as the IMAGE satellite with the same spin axis direction. We integrate the calculated line-of-sight atom flux produced by charge exchange, with the assumption of isotropic particle pressure along field lines prescribed by the T01_s plus substorm-current-wedge magnetic field model used in the simulation. Observations and simulation results for 10–60 keV hydrogen atoms agree very well, indicating the intensification and westward expansion of flux after the onsets. Although the flux intensification is partially attributed to the gradual approach of the satellite to

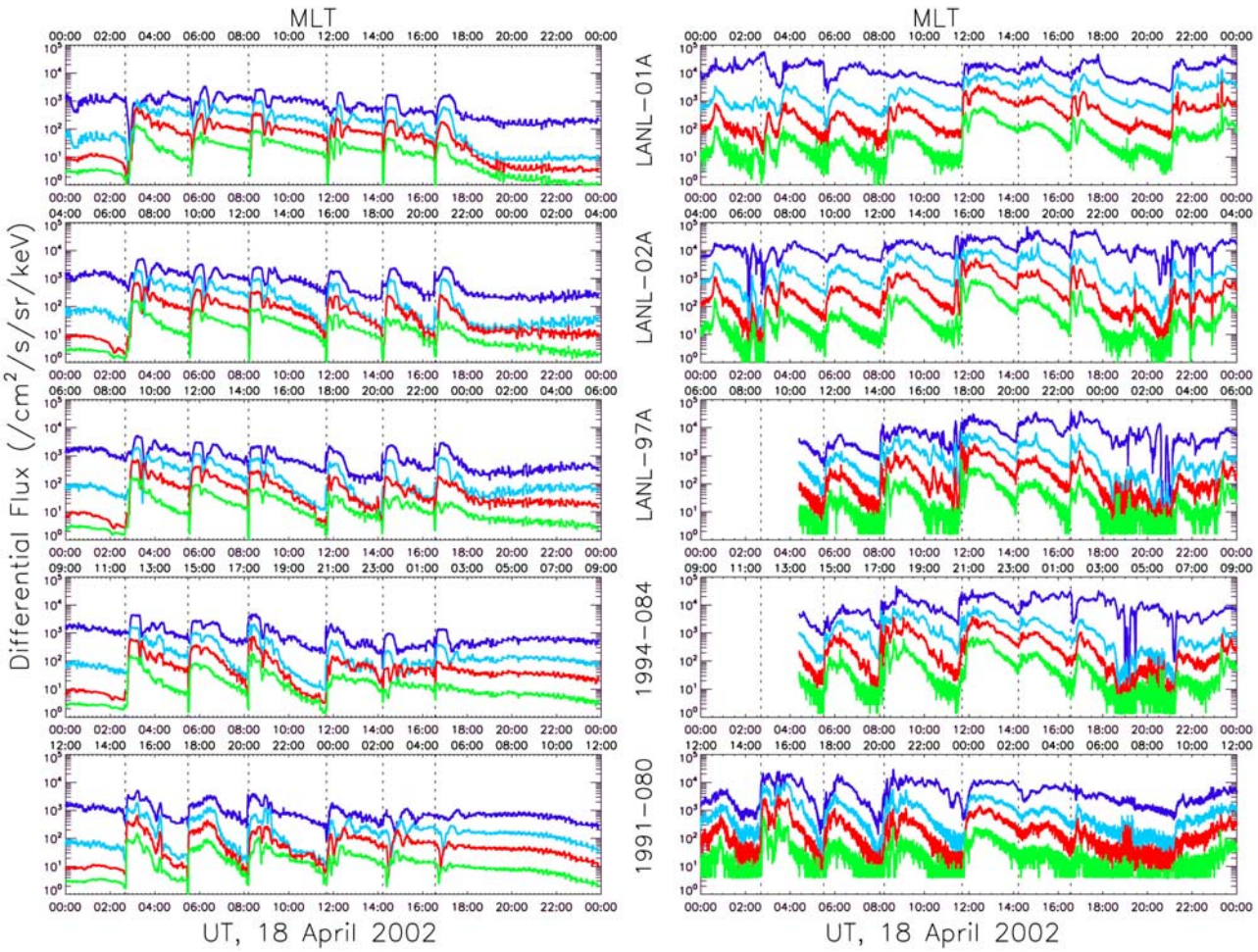


**Figure 3.** (right) The observed energetic proton flux data and (left) the corresponding simulation results for five geosynchronous satellites. The energies are 75–113, 113–170, 170–250, and 250–400 keV from blue to green. The vertical dotted lines are at the same times as in Figure 1.

the Earth, the intensification of hydrogen flux is not very pronounced. Since we assume an isotropic pitch angle distribution in our integration algorithm, the synthetic images always overestimate the flux compared to observations, especially for those lines-of-sight near the Earth. For 10–60 keV hydrogen fluxes, the observed images show the peak flux around midnight, while the simulation images indicate more duskward peaks, which implies that our simulated partial ring current shown in Figure 5 was more duskward than the real partial ring current.

[26] Figure 6 shows the computed total particle pressure of the RCM simulation for one tooth cycle. The six plots from a to f are snapshots at 0800, 0810, 0820, 0830, 0850, and 0920 UT, which approximately span the substorm growth, expansion, and recovery phases of the substorm with onset at around 0812 UT. The pressure in the growth phase is mainly attributed to the partial ring current centered in the dusk-midnight sector with peak value of 100 nPa. The pressure increases after onset and peaks at ~117 nPa 10 minutes later, after the field dipolarization and the plasma injection at local time from 1400 to 0100 MLT with low $PV^{5/3}$ [*Lemon et al.*, 2004; *Lyons et al.*, 2003]. Since the plasma pressure and flux tube volume increase tailward during steady convection, the pressure balance inconsistency [*Erickson and Wolf*, 1980] suggests that the fresh plasma cannot be injected from the magnetotail until the plasma entropy $PV^{5/3}$ is reduced by some mechanism. Reconnection could nonadiabatically cut the long flux tube into a shorter closed flux tube and a plasmoid and also generate fast earthward flows, upsetting the well established shielding of the inner and middle magnetosphere. Concomitant with interchange convection, the plasmas containing $PV^{5/3}$ as low as about 0.02 nPa $(R_e/nT)^{5/3}$ tend to inject deep to L ~ 3.5 region where the $PV^{5/3}$ is about the same as the injected plasma. Figure 2 (bottom) shows the total particle energy within the simulation region, which clearly indicates that the particle injection occurred almost immediately after every onset. The sudden energy increase at each field collapse is mainly due to (1) many plasma-populated flux tubes are suddenly transported from outside the RCM boundary to inside after each substorm onset and (2) many nightside and duskside flux tubes that were in the RCM region before the field collapse get compressed inside the substorm current wedge, raising the average energy of the particles on those tubes. The reverse process occurs between the collapses, i.e., as the field re-stretches, the amount of magnetic flux in the RCM region decreases and other tubes

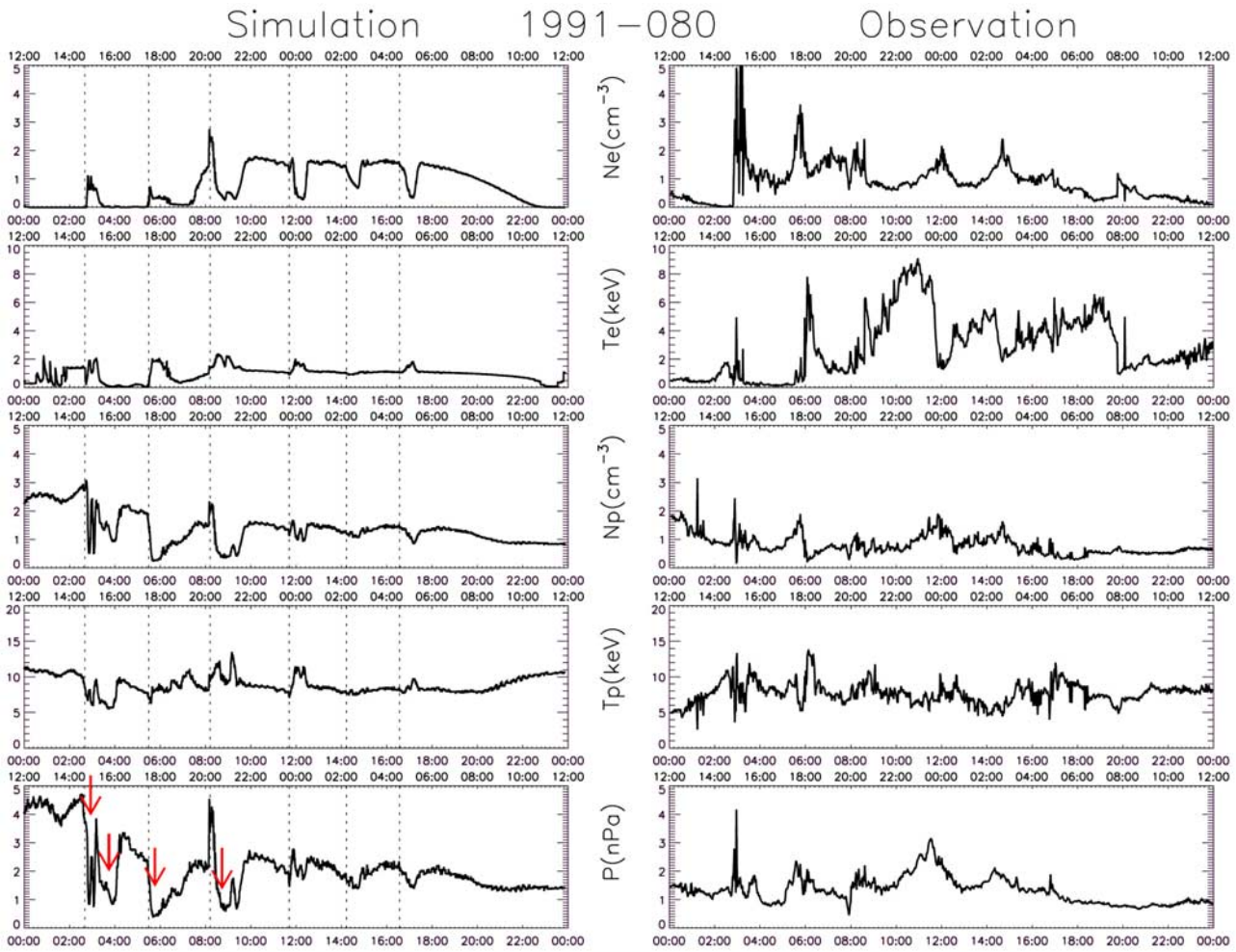


**Figure 4.** (right) The observed 1991-080 MPA data and (left) the corresponding simulated values. The electron number density $N_e$, electron temperature $T_e$, proton number density $N_p$, proton temperature $T_p$, and the particle pressure $P$ (assuming $P = k_B(T_eN_e + N_pT_p)$) are plotted from top to bottom. The red arrows indicate the times when the 1991-080 was inside the ingoing low $PV^{5/3}$ undulations.

experience an increase in volume, which de-energizes the particles on them.

### 4.3. Interchange and IMAGE/FUV Observations

[27] *Schmidt* [1979] showed the interchange criterion for two adjacent flux tubes (one with volume $V$ and pressure $P$ and the other with $V + dV$ and $P + dP$) as $dV^*dPV^{5/3} < 0$, within the assumption of ideal MHD. *Xing and Wolf* [2007] and *Erickson and Wolf* [1980] estimated $PV^{5/3}$ using empirical models and found that the inner and middle plasma sheet is generally interchange stable. However, reduction of $PV^{5/3}$ on flux tubes coming from the tail occurs during substorms [*Lyons et al.*, 2003; *Wolf et al.*, 2006a] or storms [*Sazykin et al.*, 2002], which can result in a situation where $PV^{5/3}$ decreases tailward, which would meet the criterion for interchange instability. An RCM simulation of interchange convection that was carried out for an observed storm event by *Sazykin et al.* [2002] showed that flux tubes with high $PV^{5/3}$ in the inner magnetosphere were replaced by low $PV^{5/3}$ flux tubes injected from geosynchronous orbit.

[28] The left column of Figure 7 shows the RCM simulation of the $PV^{5/3}$ distribution in the equatorial plane at times 0537, 0543, 0549, 0559 and 0617 UT on 18 April 2002. It is clear that low-$PV^{5/3}$ plasma near the boundary gets injected deep into the near-earth region at around $L$ = 3-4, while plasma of high $PV^{5/3}$ that was originally closer to Earth moves outward, producing quasi-periodic swirl patterns in electric potential and ripple-like convection cells. The interchange structure began near 0537 UT, about 7 minutes after the 0530 UT onset. The injection boundary of this tooth cycle was extremely wide, from 1400 to 0700 MLT [*Reeves et al.*, 2004], and $PV^{5/3}$ dropped from 0.030 to 0.016 nPa $(\mathrm{Re/nT})^{5/3}$ in that sector. Up to 8 interchange convection cells are visible at 0559 UT, with azimuthal width of ~25 degrees. The Vasyliunas equation

$$J_{\parallel} = \frac{\hat{b} \cdot \nabla V \times \nabla PV^{5/3}}{V^{5/3}}$$

implies that the interlacing of low and high $PV^{5/3}$ would produce quasi-periodic upward and downward field-aligned currents above the ionosphere. The middle column plots of Figure 7 show the modeled field-aligned currents mapped onto the ionosphere, with the red color representing upward

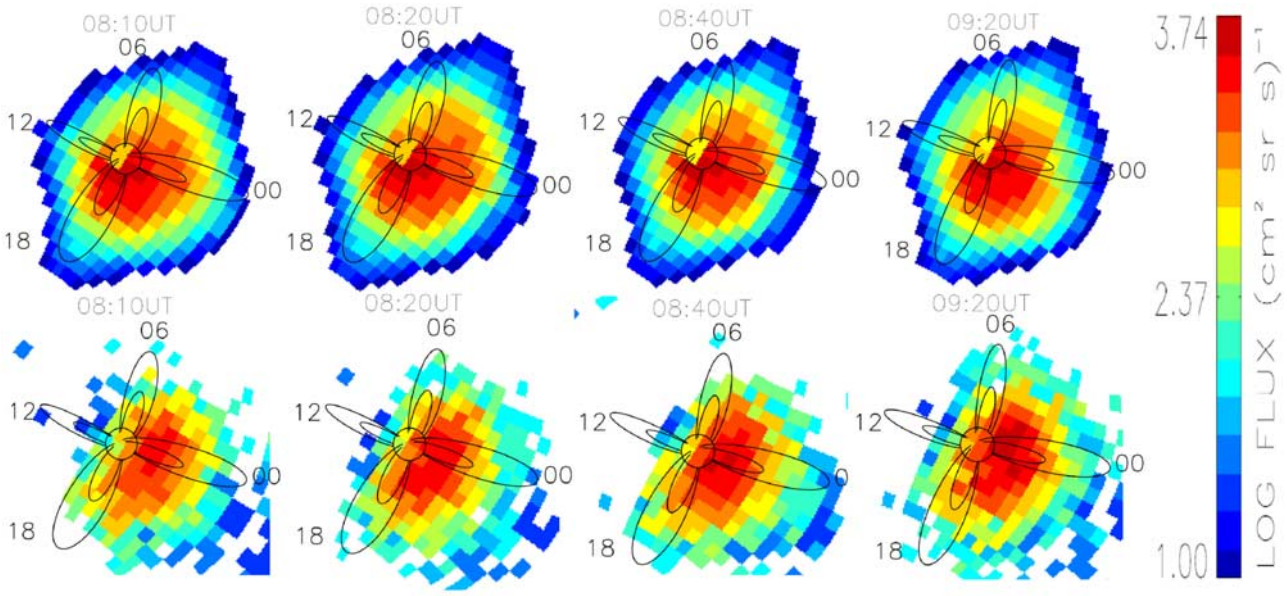


**Figure 5.** Energetic neutral atom flux of 10–60 keV hydrogen as measured by (second row) IMAGE/HENA compared with the corresponding synthetic flux from (first row) RCM simulation results. The images for times 0810, 0820, 0840, and 0920 UT are shown from left to right. The circle at the center of each image represents the Earth, and the curves are $L = 4$ and 8 dipole field lines at four local times.

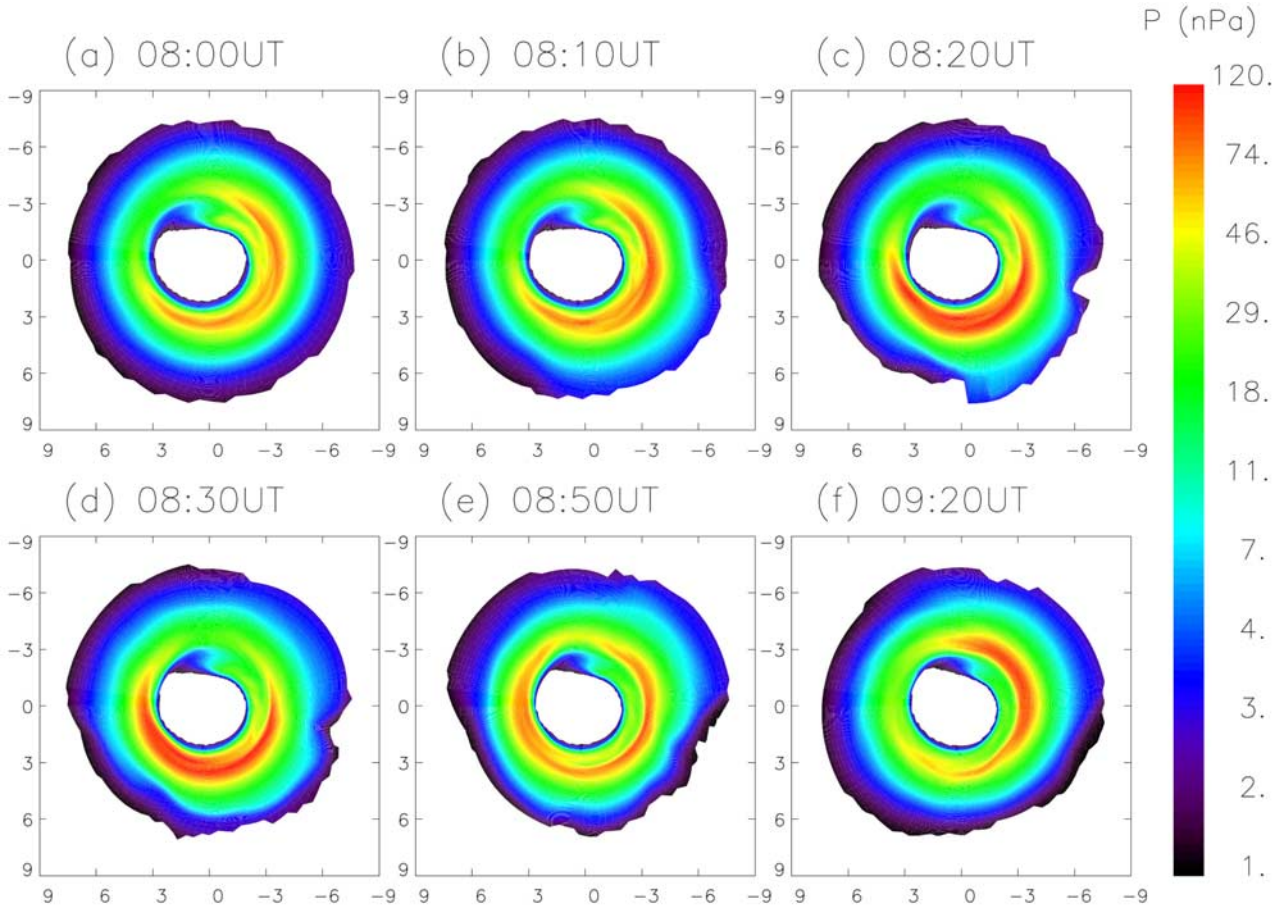


**Figure 6.** Total equatorial particle pressure for 0800, 0810, 0820, 0830, 0850, and 0920 UT. The sun is to the left.

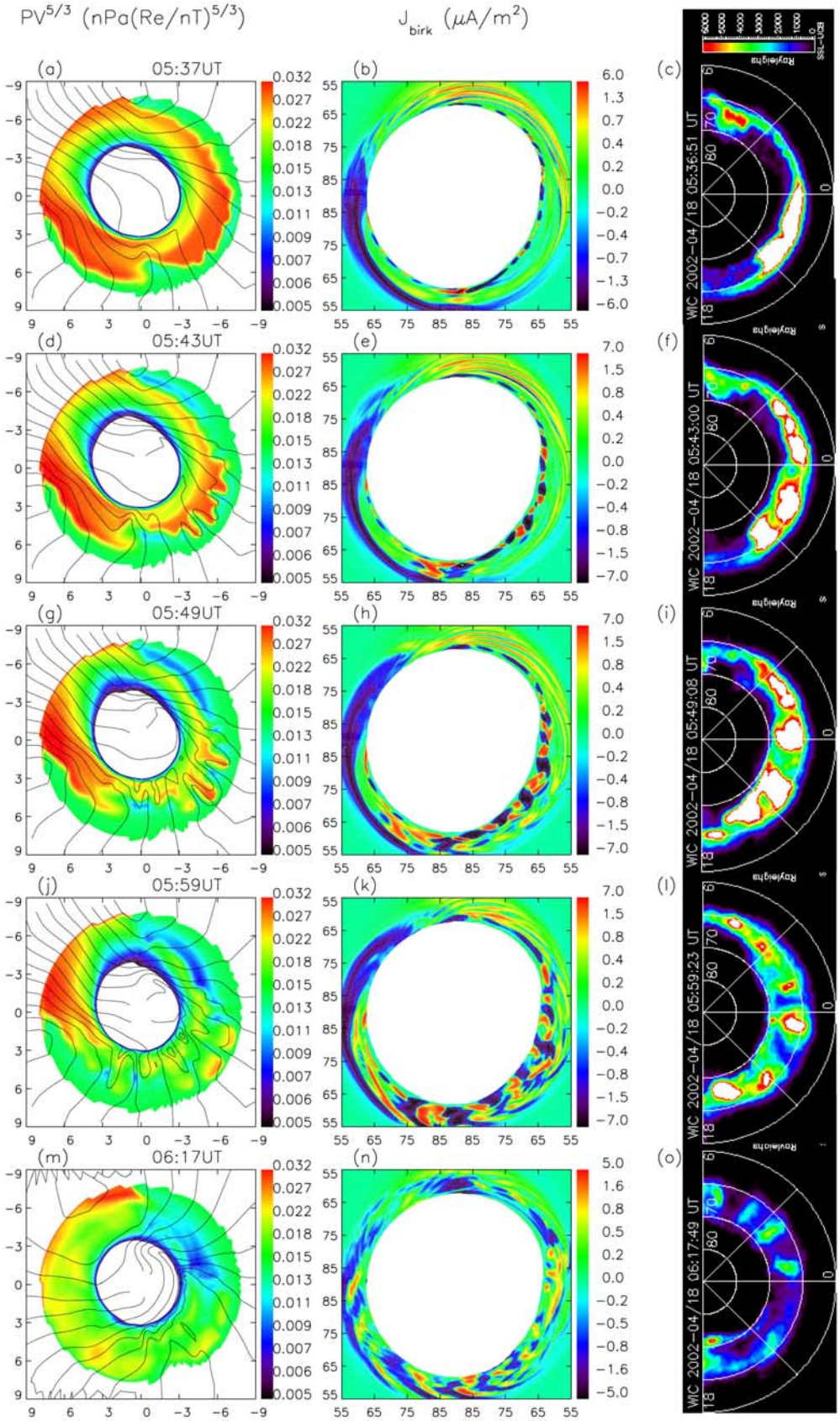


**Figure 7.** (left) The equatorial values of $PV^{5/3}$, (middle) the Birkeland current in the ionosphere, and (right) the IMAGE/FUV WIC images at times 0537, 0543, 0549, 0559, and 0617 UT from top to bottom. The sun is to the left. The solid lines shown on the left are the electric potential lines every 8 kV. Red and yellow in the middle represent upward Birkeland currents.

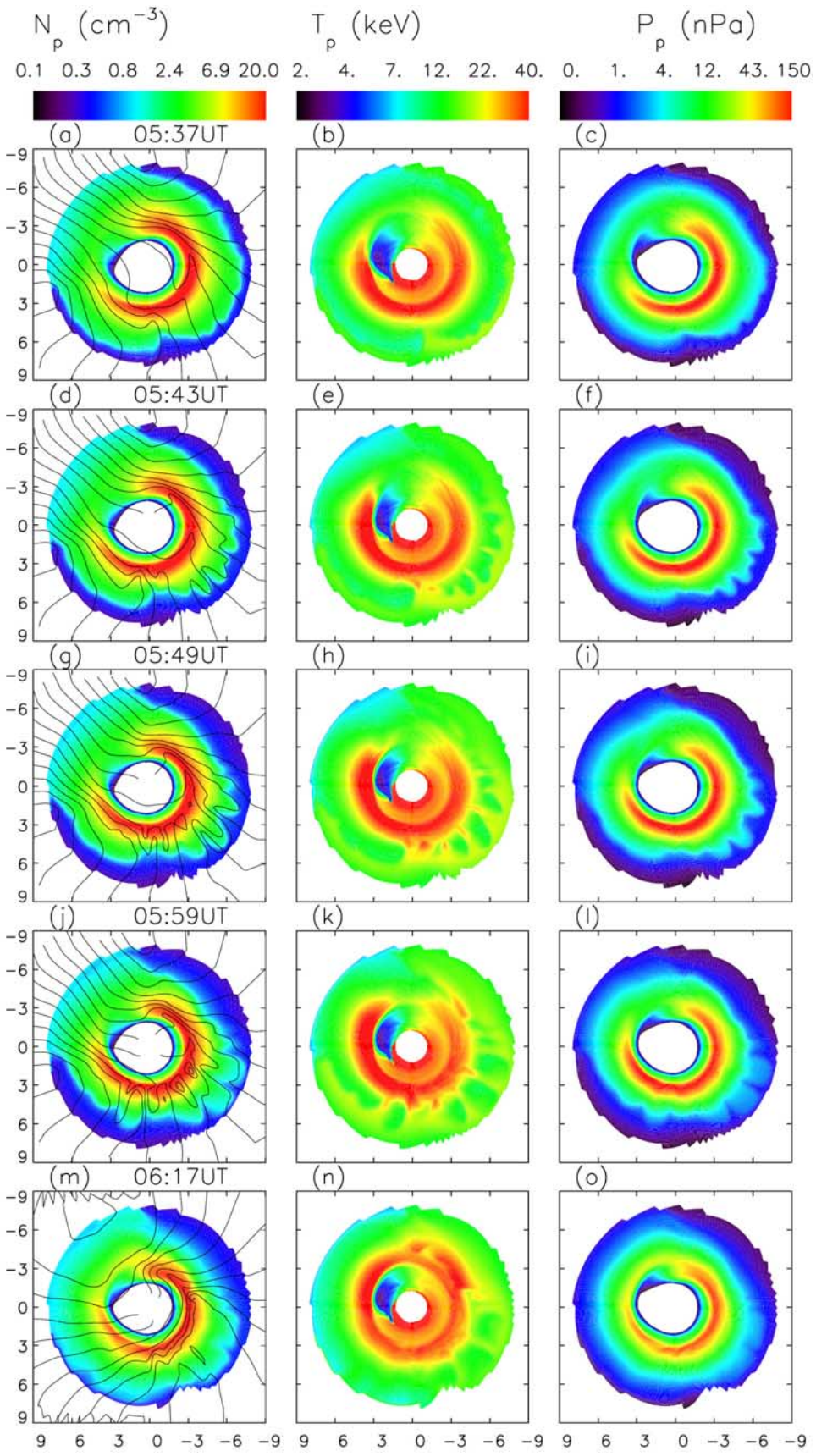


**Figure 8.** The proton number density ($N_p$) on the left, the proton temperature ($T_p$) in the middle, and the proton pressure ($P_p$) on the right at times 0537, 0543, 0549, 0559, and 0617 UT from top to bottom. The sun is to the left. The solid lines on the left are the electric potential lines every 8 kV.

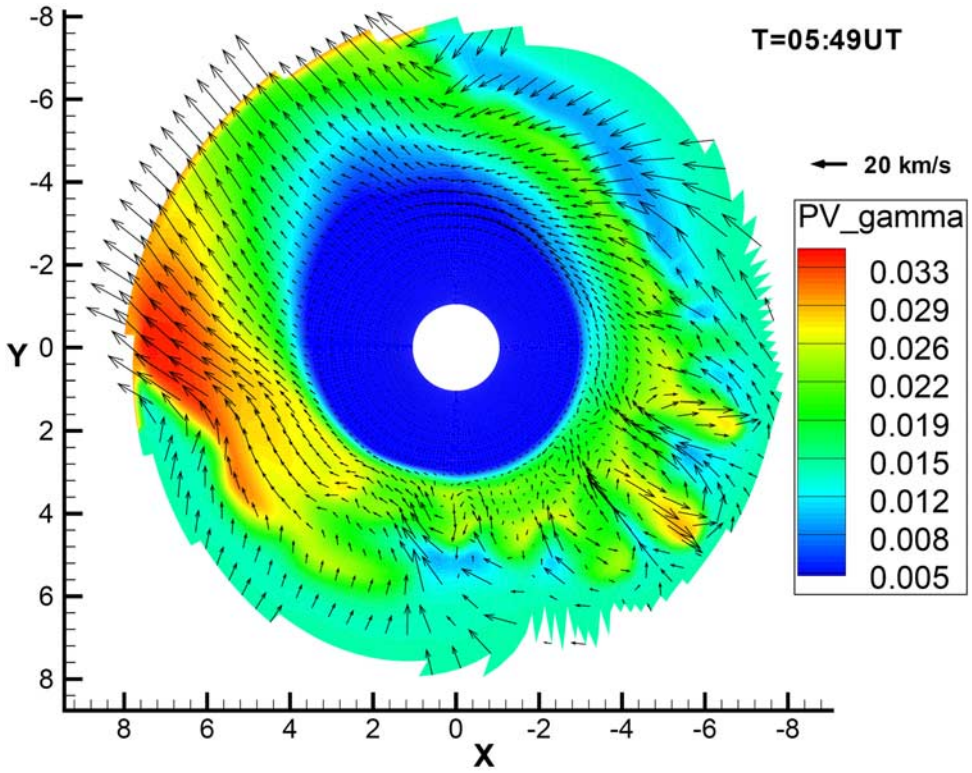


**Figure 9.** Equatorial $E \times B$ drift velocities in the potential electric field in corotating frame at time 05:49 UT. Colors represent the $PV^{5/3}$ on the equatorial plane.

currents. A close view of a specific current footprint indicates that regions of both upward and downward currents grow and move equatorward and westward. The IMAGE/FUV WIC observed quasi-periodic and westward drifting auroral structures during this event [*Ohtani et al.*, 2007]. The plots on the right column of Figure 7 show the WIC snapshots closest to the times at 0537, 0543, 0549, 0559 and 0617 UT, but only nightside images are shown to avoid air glow contamination on the dayside. The auroral arcs brighten first in the midnight sector, and then grow to a spatial periodic structure covering the whole nightside. At about 0559 UT, they stretch out to an almost north–south-aligned finger-like structure, very similar to the simulation results. We suggest that this auroral pattern is associated with the strong periodic field-aligned current caused by interchange, because strong electron aurora tend to occur in regions of strong upward field-aligned current. Figure 8 clearly shows how plasma moments of protons change for this period. Low-number-density, high-temperature plasma is injected along a wide section of the RCM boundary and drifts into the inner magnetosphere, producing quasi-periodic spatial distributions there. Flux tubes carrying relatively low thermal pressure and $PV^{5/3}$ from the boundary could penetrate inside geosynchronous orbit. According to the model, the virtual 1991–080 satellite was just inside the inflowing $PV^{5/3}$ plasma in the dusk to pre-midnight sector for four periods at around 03:00, 03:50, 05:50 and 0830 UT as indicated by the red arrows in the simulated MPA proton pressure in Figure 4.

[29] The electric field plays an important role in the plasma injection. As indicated in Figure 9, the self-consistently computed electric potential electric field swirls tend to produce almost azimuthal electric field, which drives $E \times B$ drift mainly in the radial direction, with low $PV^{5/3}$ plasma moving inward and high $PV^{5/3}$ plasma moving outward. This pattern helps the interchange-unstable system to reconfigure itself to a stable state.

[30] Actually, the simulation indicates that the interchange instability and the concurrent periodic upward-downward Birkeland currents occur in every tooth cycle. These auroral structures have been identified by eye, with no rigorous morphological criterion applied. In general, the RCM results produce 4–8 coupled pairs of downward-upward Birkeland currents with averaged spatial periodicity of 1.5 hours to 2.0 hours local time and lifetime of 40–60 minutes, while the IMAGE observation shows 3–7 auroral fingers with average spatial periodicity of 1.5 to 1.8 hours in local time and lifetime 20–75 minutes. Note that the first tooth cycle was actually observed to be more complicated, because it was a double-onset event [*Clauer et al.*, 2006], but our simulation set up only one injection for that period. The average spatial periodicity of 1.5–2.0 hours of these finger-like auroral structures implies that the reduction of $PV^{5/3}$ on an unusual wide local time is important in the formation of several concurrent interchange convection cells in the sawtooth event. This suggests that the dynamic reconfiguration of magnetic field and plasma during sawtooth events may provide optimal conditions for interchange instability. *Sazykin et al.* [2002] used plasma data at geosynchronous orbit to set up boundary conditions during a storm, producing interchange convection in the inner magnetosphere, which was also during a sawtooth event on 25 September 1998. As far as we know, there are no direct *in situ* observations reported regarding interchange convec-

tion in the magnetosphere. Coordinated satellite observations might be used to investigate one or several of the following features associated with interchange convection: swirl-like electric potential, radially moving plasma, interlacing high- and low- plasma entropy parameter $PV^{5/3}$ [*Wolf et al.*, 2006b]. It is also important to note that the choice of RCM grid spacing influences the computed number and scale size of fingers; for example an RCM run with a finer longitudinal grid increases the number of fingers, so a one-to-one comparison between RCM results and observations should be interpreted with some degree of skepticism. A careful study of the dependence of the properties of the interchange fingers and numerical resolution could be the subject of future study.

[31] The reader may note that the observed quasi-periodic auroral structures appear to extend to nearly 70° magnetic latitude, while the corresponding RCM structures are confined to the region equatorward of the model boundary, which is at about 65°. If we had placed the boundary further out in the tail, the modeled interchange fingers would have extended further poleward. However, since the fingers arise in periods when the magnetic field is significantly dipolarized, the 70° magnetic latitude may not map too far out in the tail. Mapping along our event-specific magnetic field model, the equatorial crossings of the 70 degree magnetic latitude points are approximately 11.9, 11.8, and 10.3 $R_e$ in the pre-midnight sector after the first three substorm onsets, respectively.

[32] It should also be noted that none of the previous modeling papers on this event, mentioned in section 1, show clear evidence of interchange instability in the inner magnetosphere. The pure-MHD paper of *Goodrich et al.* [2007] and the modified-MHD paper of *Kuznetsova et al.* [2007] do not present any detail about the inner magnetosphere. *Taktakishvili et al.* [2007] does emphasize the inner magnetosphere, and the results do not seem to show any evidence of interchange instability there. It is not clear why there is such a difference between the predictions of the models. Of course, one way in which the RCM differs from the others is that its plasma boundary condition is set from observations rather than pure theory. The reason for the discrepancy also may lie in numerical diffusion in the MHD code. The Fok code resolves the inner magnetosphere well but is limited by its use of MHD-computed electric fields. Our approach is to use the RCM to provide a detailed picture of the ring current, but using a Tsyganenko magnetic field model tuned for the event and potential electric fields that are computed self-consistently with the inner-magnetosphere particles. This active particle-field coupling in the RCM produces electric fields and Birkeland currents that are quite different from the results of the BATS-R-US/Fok simulation. RCM grid spacing and numerical method are, of course, specifically designed for resolving inner-magnetospheric processes, and it computes its potential electric field self-consistently.

## 5. Conclusions

[33] We have simulated the 18 April 2002 sawtooth event using the Rice Convection Model with inputs carefully adjusted to give optimum agreement with observational data. The T01_s magnetic field model, augmented by a modified Tsyganenko substorm current wedge model, was adjusted for approximate consistency with the magnetic field measured at geosynchronous orbit. The six tooth oscillations were treated as six substorms with broad injection fronts. Therefore substorm-related processes, i.e., strong stretching and dipolarization of magnetic field, intense ionosphere outflows and reconnection and plasmoid formation in the magnetotail, were taken into consideration by imposing different plasma distributions on the simulation boundary at $-8$ $R_e$ during different substorm phases.

[34] 1. We were able to match the simulated energetic proton fluxes with LANL/SOPA observed flux oscillations, i.e., rapid increase after every substorm onset, globally and without prominent dispersion, and gradual decrease thereafter. Our modeling implies that highly elevated SOPA fluxes require up to ~25 keV temperature plasma boundary condition in the near-Earth region after every onset. We suggest that the temperature enhancement would be attributed to the acceleration because of the induction electric field when the magnetic field collapses strongly in an unusually wide local time range during the sawtooth event.

[35] 2. The simulated energetic neutral atom fluxes are consistent with the IMAGE/HENA fluxes for 10–60 keV hydrogen. The ring current pressure peaks around 10–20 minutes after every onset. We believe that the intensification of ring current is associated with the injection of plasma of low $PV^{5/3}$.

[36] 3. Our simulation produced interchange convection cells with lifetimes of 40–60 minutes and average spatial periodicity of 1.5–2.0 hours in local time and corresponding 4–8 pairs of downward-upward field-aligned currents, although the exact details of the interchange pairs appears to be dependent on numerical resolution and will be left for future work. However, this interchange pattern is consistent with quasi-periodic finger-like north–south-aligned auroral structures observed in IMAGE/FUV WIC images in both spatial and temporal scales. We suggest that this spatially periodic interchange pattern naturally occurs when the large $PV^{5/3}$ reduction happens over a wide range of local time.

## Appendix A: Set-up of Substorm Current Wedge Model

[37] The Tsyganenko substorm current wedge model [*Tsyganenko*, 1997] is a simple analytic magnetic field model describing the current distribution and the corresponding magnetic field disturbance after substorm onset. The model applies a pair of current loops with a spread-out volume current density to represent the geometry and magnitude to the substorm current wedge [*McPherron et al.*, 1973]. The original code provided by Tsyganenko consists of five free parameters to adjust, i.e., "AMPL," wedge amplitude coefficient, to specify the magnitude of the current; "R0," loop initial radius; "AL," loop stretch amplitude; "BETA," loop extension amplitude; "GAMMA," loop inclination angle with respect to equatorial plane in radians. The definition of these parameters can be found in equations (1), (2), and (3) of *Tsyganenko* [1997]. The last five figures in Figure A1 show the five parameters used in our simulation versus time. Basically, AMPL = 100 yields about +10 to +20 nT disturbance inside the wedge; R0, AL and BETA describe the geometry of the pair of current

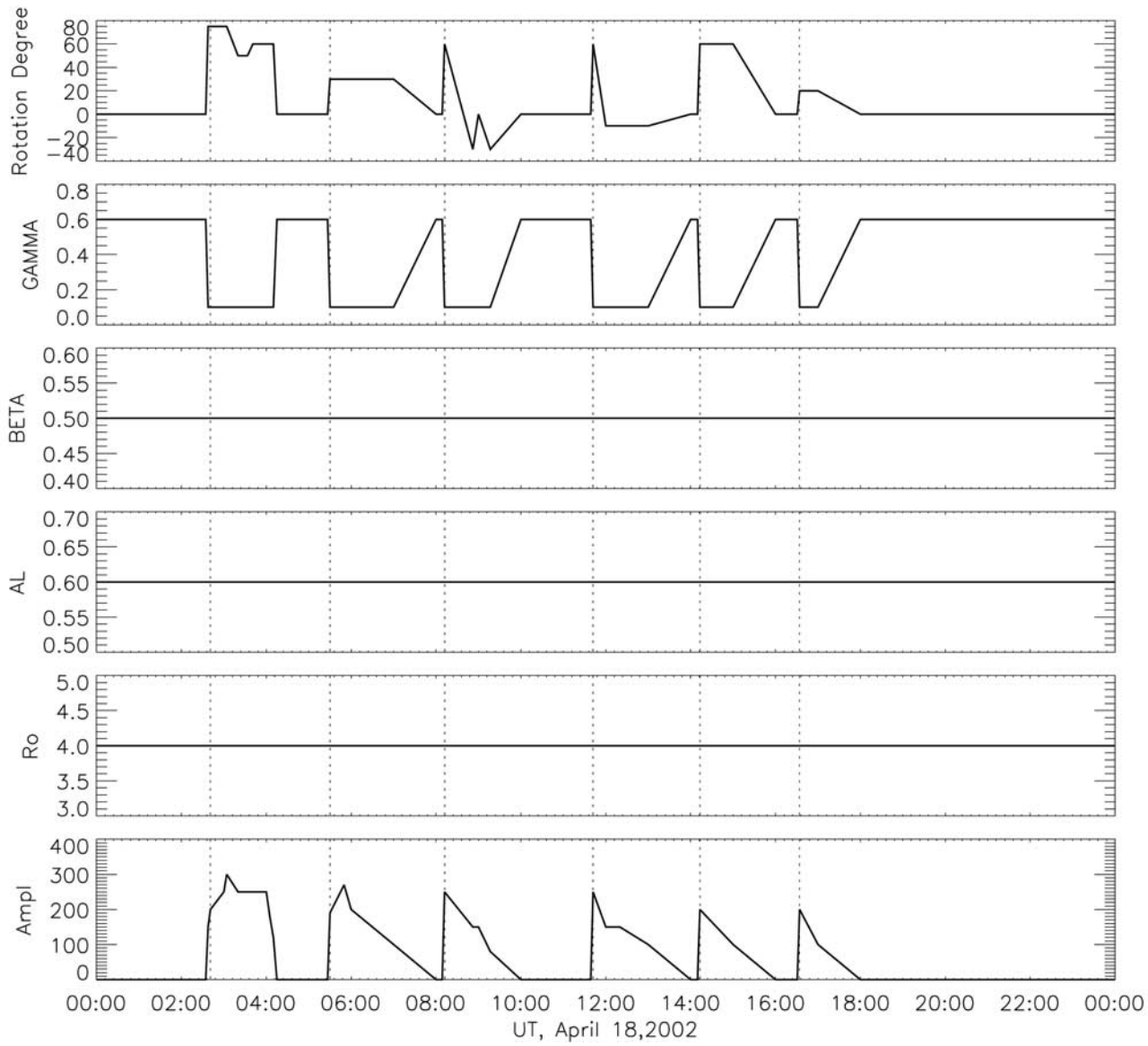


**Figure A1.** Six parameters of the substorm current wedge model in this run versus time. The vertical dotted lines are at the same times as in Figure 1.

loops, which remain unchanged throughout the run; The inclination angle of the loop with respect to the equatorial plane, i.e., GAMMA, is changing. The original substorm current wedge model assumes that the wedge is always centered at midnight, which is not the case in this event. Both the magnetic field disturbances recorded by ground magnetometers [*Clauer et al.*, 2006] and SOPA energetic particle flux analysis [*Reeves et al.*, 2004] suggest that the substorm current wedge is centered at local times varying from close to the dusk terminator to near midnight. Therefore we introduce a new parameter ''Rotation Degree'' to be able to rotate the whole structure of the Tsyganenko substorm current wedge about the dipolar axis. The top of Figure A1 shows this parameter versus time where a positive angle represents a westward rotation. It is clear that for most of the time, the current wedge is centered in the dusk-midnight sector. To best match the dipolarizations observed by GOES 8 and GOES 10 during this event and for technical simplicity, we tune only three parameters of the current wedge model, ''AMPL,'' ''GAMMA'' and ''Rotation Degree,'' keeping the other three parameters unchanged. Obviously, ''AMPL'' also shows sawtooth-like oscillations, because the current magnitude is strong after every onset and then gradually decreases to zero in the late recovery phase and the next growth phase.

[38] **Acknowledgments.** We thank N. A. Tsyganenko for providing the substorm current wedge model source code. We are also grateful to C.-S. Huang, G. D. Reeves, and M. F. Thomsen for helpful discussions. The Dst indices and Kp indices were provided by the World Data Center for Geomagnetism, Kyoto. The Wind, GOES 8 and GOES 10 data were obtained through SPIDR. This work was supported by NASA Guest Investigator grant NNG05GE36G, by the National Space Weather Program under NSF grant ATM-0720309, and by the NASA Heliospheric Theory Program under grant NNG05GH93G. Work by P. C. Brandt at the Applied Physics Laboratory was supported by NASA grant NNX06AC29G.

[39] Wolfgang Baumjohann thanks Richard L. Kaufmann and another reviewer for their assistance in evaluating this paper.

## References


Baumjohann, W., G. Paschmann, and C. A. Cattell (1989), Average plasma properties in the central plasma sheet, *J. Geophys. Res.*, *94*, 6597–6606.

Belian, R. D., T. E. Cayton, and G. D. Reeves (1995). Quasi-periodic global substorm-generated variations observed at geosynchronous orbit, in *Space Plasmas: Coupling Between Small and Medium Scale Processes*, *Geophys. Monogr. Ser.*, vol. 86, p. 143, AGU, Washington, D. C.

Borovsky, J. E., R. J. Nemzek, and R. D. Belian (1993), The occurrence rate of magnetospheric-substorm onsets: Random and periodic substorms, *J. Geophys. Res.*, *98*, 3807–3813.

Borovsky, J. E., M. F. Thomsen, R. C. Elphic, T. E. Cayton, and D. J. McComas (1998), The transport of plasma sheet material from the distant tail to geosynchronous orbit, *J. Geophys. Res.*, *103*, 20,297–20,331.

Boyle, C. B., P. H. Reiff, and M. R. Hairston (1997), Empirical polar cap potentials, *J. Geophys. Res.*, *102*, 111–125.

Clauer, C. R., X. Cai, D. Welling, A. DeJong, and M. G. Henderson (2006), Characterizing the 18 April 2002 storm-time sawtooth events using ground magnetic data, *J. Geophys. Res.*, *111*, A04S90, doi:10.1029/2005JA011099.

Daglis, I. A., S. Livi, E. T. Sarris, and B. Wilken (1994), Energy density of ionospheric and solar wind origin ions in the near-Earth magnetotail during substorms, *J. Geophys. Res.*, *99*, 5691–5704.

Delcourt, D. C. (2002), Particle acceleration by inductive electric fields in the inner magnetosphere, *J. Atmos. Sol. Terr. Phys.*, *64*, 551–559.

Erickson, G. M., and R. A. Wolf (1980), Is steady convection possible in the Earth's magnetotail?, *Geophys. Res. Lett.*, *7*, 897–900.

Fujimoto, M., T. Terasawa, T. Mukai, Y. Saito, T. Yamamoto, and S. Kokubun (1998), Plasma entry from the flanks of the near-Earth magnetotail: Geotail observations, *J. Geophys. Res.*, *103*, 4391–4408.

Henderson, M. G. (2004), The May 2–3, 1986 CDAW-9C interval: A sawtooth event, *Geophys. Res. Lett.*, *31*, L11804, doi:10.1029/2004GL019941.

Henderson, M. G., G. D. Reeves, R. Skoug, M. T. Thomsen, M. H. Denton, S. B. Mende, T. J. Immel, P. C. Brandt, and H. J. Singer (2006), Magnetospheric and auroral activity during the 18 April 2002 sawtooth event, *J. Geophys. Res.*, *111*, A01S90, doi:10.1029/2005JA011111.

Hones, E. W., Jr. (1977), Comments on "On hot, tenuous plasmas, fireballs, and boundary layers in the Earth's magnetotail," by L. A. Frank, K. L. Ackerson, and R. P. Lepping, *J. Geophys. Res.*, *82*, 5633–5640.

Huang, C.-S., G. D. Reeves, J. E. Borovsky, R. M. Skoug, Z. Y. Pu, and G. Le (2003a), Periodic magnetospheric substorms and their relationship with solar wind variations, *J. Geophys. Res.*, *108*(A6), 1255, doi:10.1029/2002JA009704.

Huang, C.-S., J. C. Foster, G. D. Reeves, G. Le, H. U. Frey, C. J. Pollock, and J.-M. Jahn (2003b), Periodic magnetospheric substorms: Multiple space-based and ground-based instrumental observations, *J. Geophys. Res.*, *108*(A11), 1411, doi:10.1029/2003JA009992.

Goodrich, C. C., T. I. Pulkkinen, J. G. Lyon, and V. G. Merkin (2007), Magnetospheric convection during intermediate driving: Sawtooth events and steady convection intervals as seen in Lyon-Fedder-Mobarry global MHD simulations, *J. Geophys. Res.*, *112*, A08201, doi:10.1029/2006JA012155.

Kaufmann, R. L., and W. R. Paterson (2006), Magnetic flux and particle transport in the plasma sheet, *J. Geophys. Res.*, *111*, A10214, doi:10.1029/2006JA011734.

Kuznetsova, M. M., M. Hesse, L. Rastatter, A. Taktakishvili, G. Toth, D. L. De Zeeuw, A. Ridley, and T. I. Gombosi (2007), Multiscale modeling of magnetospheric reconnection, *J. Geophys. Res.*, *112*, A10210, doi:10.1029/2007JA012316.

Lee, D.-Y., L. R. Lyons, and K. Yumoto (2004), Sawtooth oscillations directly driven by solar wind dynamic pressure enhancements, *J. Geophys. Res.*, *109*, A04202, doi:10.1029/2003JA010246.

Lemon, C., R. A. Wolf, T. W. Hill, S. Sazykin, R. W. Spiro, F. R. Toffoletto, J. Birn, and M. Hesse (2004), Magnetic storm ring current injection modeled with the Rice Convection Model and a self-consistent magnetic field, *Geophys. Res. Lett.*, *31*, L21801, doi:10.1029/2004GL020914.

Lui, A. T. Y., R. E. Lopez, B. J. Anderson, K. Takahashi, L. J. Zanetti, R. W. McEntire, T. A. Potemra, D. M. Klumpar, E. M. Greene, and R. Strangeway (1992), Current disruptions in the near-earth neutral sheet region, *J. Geophys. Res.*, *97*, 1461–1480.

Lyons, L. R., C.-P. Wang, T. Nagai, T. Mukai, Y. Saito, and J. C. Samson (2003), Substorm inner plasma sheet particle reduction, *J. Geophys. Res.*, *108*(A12), 1426, doi:10.1029/2003JA010177.

Mauk, B. H., and C. I. Meng (1983), Characterization of geostationary particle signatures based on the "injection boundary" model, *J. Geophys. Res.*, *88*, 3055–3071.

McPherron, R. L., C. T. Russell, and M. P. Aubry (1973), Satellite studies of magnetospheric substorms on August 15, 1968: 9. Phenomenological model for substorms, *J. Geophys. Res.*, *78*, 3131–3149.

Ohtani, S., et al. (2007), Cluster observations in the inner magnetosphere during the 18 April 2002 sawtooth event: Dipolarization and injection at $r = 4.6$ RE, *J. Geophys. Res.*, *112*, A08213, doi:10.1029/2007JA012357.

Pulkkinen, T. I., N. Y. Ganushkina, E. I. Tanskanen, M. Kubyshkina, G. D. Reeves, M. F. Thomsen, C. T. Russell, H. J. Singer, J. A. Slavin, and J. Gjerloev (2006), Magnetospheric current systems during stormtime sawtooth events, *J. Geophys. Res.*, *111*, A11S17, doi:10.1029/2006JA011627.

Reeves, G. D., M. F. Thomsen, J. E. Borovsky, M. G. Henderson, and R. M. Skoug (2004), Sawtooth injection and the extension of substorm effects to the day side, paper presented at International Conference on Substorms (ICS-7), Lapland, Finland, 21–27 March.

Sazykin, S., R. A. Wolf, R. W. Spiro, T. I. Gombosi, D. L. De Zeeuw, and M. F. Thomsen (2002), Interchange instability in the inner magnetosphere associated with geosynchronous particle flux decreases, *Geophys. Res. Lett.*, *29*(10), 1448, doi:10.1029/2001GL014416.

Schmidt, G. (1979), *Physics of High Temperature Plasmas*, Elsevier, New York.

Shue, J.-H., et al. (1998), Magnetopause location under extreme solar wind conditions, *J. Geophys. Res.*, *103*, 17,691–17,700.

Taktakishvili, A., M. M. Kuznetsova, M. Hesse, M.-C. Fok, L. Rastatter, M. Maddox, A. Chulaki, T. I. Gombosi, and D. L. De Zeeuw (2007), Buildup of the ring current during periodic loading-unloading cycles in the magnetotail driven by steady southward interplanetary magnetic field, *J. Geophys. Res.*, *112*, A09203, doi:10.1029/2007JA012317.

Toffoletto, F. R., S. Sazykin, R. W. Sprio, and R. A. Wolf (2003), Inner magnetospheric modeling with the Rice Convection model, *Space Sci. Rev.*, *107*, 175.

Tsyganenko, N. A. (1997), An empirical model of the substorm current wedge, *J. Geophys. Res.*, *102*, 19,935–19,941.

Tsyganenko, N. A. (2002a), A model of the magnetosphere with a dawn-dusk asymmetry: 1. Mathematical structure, *J. Geophys. Res.*, *107*(A8), 1179, doi:10.1029/2001JA000219.

Tsyganenko, N. A. (2002b), A model of the near magnetosphere with a dawn-dusk asymmetry: 2. Parameterization and fitting to observations, *J. Geophys. Res.*, *107*(A8), 1176, doi:10.1029/2001JA000220.

Tsyganenko, N. A., and T. Mukai (2003), Tail plasma sheet models derived from Geotail particle data, *J. Geophys. Res.*, *108*(A3), 1136, doi:10.1029/2002JA009707.

Tung, Y.-K., C. W. Carlson, J. P. McFadden, D. M. Klumpar, G. K. Parks, W. J. Peria, and K. Liou (2001), Auroral polar cap boundary ion conic outflow observed on FAST, *J. Geophys. Res.*, *106*, 3603–3614.

Wilson, G. R., D. M. Ober, G. A. Germany, and E. J. Lund (2004), Nightside auroral zone and polar cap ion outflow as a function of substorm size and phase, *J. Geophys. Res.*, *109*, A02206, doi:10.1029/2003JA009835.

Wing, S., J. W. Gjerloev, J. R. Johnson, and R. A. Hoffman (2007), Substorm plasma sheet ion pressure profiles, *Geophys. Res. Lett.*, *34*, L16110, doi:10.1029/2007GL030453.

Wolf, R. A. (1983), The quasi-static (slow-flow) region of the magnetosphere, in *Solar Terrestrial Physics*, edited by R. L. Carovillano and J. M. Forbes, pp. 303–368, Series, D. Reidel, Hingham, Mass.

Wolf, R. A., R. W. Spiro, S. Sazykin, F. R. Toffoletto, P. L. Sager, and T. S. Huang (2006a), Use of Euler potentials for describing magnetosphere-ionosphere coupling, *J. Geophys. Res.*, *111*, A07315, doi:10.1029/2005JA011558.

Wolf, R. A., V. Kumar, F. R. Toffoletto, G. M. Erickson, A. M. Savoie, C. X. Chen, and C. L. Lemon (2006b), Estimating local plasma sheet PV 5/3 from single-spacecraft measurements, *J. Geophys. Res.*, *111*, A12218, doi:10.1029/2006JA012010.

Xing, X., and R. A. Wolf (2007), Criterion for interchange instability in a plasma connected to a conducting ionosphere, *J. Geophys. Res.*, *112*, A12209, doi:10.1029/2007JA012535.

Yau, A. W., P. H. Beckwith, W. K. Peterson, and E. G. Shelley (1985), Long-term (solar cycle) and seasonal variations of upflowing ionospheric ion events at DE1 altitudes, *J. Geophys. Res.*, *90*, 6395–6407.



P. C. Brandt, Applied Physics Laboratory, Johns Hopkins University, 11100, John Hopkins Rd., Laurel, MD 20723–6099, USA.

H. U. Frey, Space Sciences Laboratory, University of California, Berkeley, CA 94720–7450, USA.

M. G. Henderson, Los Alamos National Laboratory, MS D-466, Los Alamos, NM 87545, USA.

S. Sazykin, R. W. Spiro, F. R. Toffoletto, R. A. Wolf, and J. Yang, Department of Physics and Astronomy, Rice University, 6100 Main Street, MS-108, Houston, TX 77005, USA. (jianyang@rice.edu)